The International Journal of
Robotics Research
http://ijr.sagepub.com/

Motion control of magnetized Tetrahymena pyriformis cells by magnetic field with Model Predictive Control

Yan Ou, Dal Hyung Kim, Paul Kim, Min Jun Kim and A. Agung Julius

The International Journal of Robotics Research published online 23 October 2012
DOI: 10.1177/0278364912464669

The International Journal of
Robotics Research
0(0) 1–11

DOI: 10.1177/0278364912464669
ijr.sagepub.com

Motion control of magnetized *Tetrahymena pyriformis* cells by a magnetic field with Model Predictive Control

Yan Ou[1], Dal Hyung Kim[2], Paul Kim[2], Min Jun Kim[2] and A Agung Julius[1]

Abstract

This paper presents the Model Predictive Control (MPC) of magnetized Tetrahymena pyriformis (T. pyriformis) using a magnetic field. The magnetized T. pyriformis are generated by feeding spherical iron oxide particles into the cells. Using an external magnetic field, we change the movement direction of the cell, but the speed of the cell remains constant regardless of the strength of the external magnetic field. The contributions of this paper are threefold. First, the discrete-time plant model of the magnetized cell is generated using the least-squares method. Second, using the model of each cell, they are controlled to follow a reference track by an external magnetic field with MPC. Third, by using a predictor-like scheme to execute the plant input before the measurement of the cell position, we successfully solve the image-processing delay problem in the feedback system. In our results, we show three comparisons between different control schemes and an initial tracking to prove the effectiveness of the control approach.

Keywords

Magnetotaxis, microrobots, model predictive control, motion control, time delay, *Tetrahymena pyriformis*

1. Introduction

The control of microrobots is a novel research area and has many applications, for example, microdelivery (Martel 2006), parallel assembly (Donald et al. 2008), and micromanipulation Hunter et al. (1990). Among the existing work in this field, the main focus has been on developing artificial microrobots (Martel et al. 2006; Abbott et al. 2007; Martel et al. 2009; Pawashe et al. 2009; Zhang et al. 2009). Compared with microorganisms, artificial microrobots are easier to control because the plant model is easier to identify and contains less uncertainty. Artificial microrobots can be actuated by multiple power sources. However, there are two main challenges: one is the high cost; the other is the difficulty in supplying sufficient power to artificial microrobots in a microfludic environment.

Microorganisms (Itoh 2000; Yi et al. 2000; Itoh et al. 2005), such as *Escherichia coli*, *Serratia marcescens*, and *T. pyriformis*, are easy and cheap to produce Julius et al. (2009). The biomolecular motor, like flagellum which is embedded in microorganisms, generates a swimming force by consuming chemical energy in the fluidic environment. Accordingly, several researchers have begun to use multiple stimuli to propel microorganisms as *microbiorobots*.

Currently, controlling swarms of prokaryotic cells, especially bacteria, as microbiorobots attracted major attention among researchers. For example, Martel et al. (2006) used magnetotactic bacteria to manipulate microobjects, and Sakar et al. (2010) described the construction and operation of truly microsized, biocompatible ferromagnetic microtransporters driven by external magnetic fields. Steager et al. (2011) used ultraviolet light and current electric fields to control the rotation and movement of a microbiorobot that was covered with the bacterium *S. marcescens*, and Julius et al. (2009) developed a model for a microstructure blotted with bacteria moving in a microchannel propelled by the flagella of the bacteria.

There are also some researchers focusing on controlling eukaryotic cells as microbiorobots. Normally, the size of eukaryotic cells is much larger than that of prokaryotic cells. This property makes it easy for us to generate the plant model and measure the positions of a single eukaryotic cell. Fearing (1991) used electrodes to investigate the control of *Paramecium* as a prototypical microrobot and Weibel et al. (2005) demonstrated the biological propulsion of microscale loads by the unicellular photosynthetic algae

[1]Department of Electrical, Computer, and Systems Engineering, Rensselaer Polytechnic Institute, USA
[2]Department of Mechanical Engineering and Mechanics, Drexel University, USA

Corresponding author:
Yan Ou, Department of Electrical, Computer, and Systems Engineering, Rensselaer Polytechnic Institute, 110 8th Street, Troy, NY 12180, USA.
Email: ouy2@rpi.edu

Chlamydomonas reinhardtii. Itoh and Toida (2001) aimed to control bioconvection by applying an electrical field and then applying this bioconvection as an energy or mechanical power source.

Tetrahymena pyriformis (*T. pyriformis*) is a eukaryotic pear-shaped cell of size 50 μm long and 25 μm wide. The body of *T. pyriformis* is covered by approximately 600 oral or locomotive cilia. The locomotive cilia facilitate the swimming behavior of *T. pyriformis*, which can be influenced by external stimuli, such as magnetotaxis, chemotaxis, phototaxis, aerotaxis, galvanotaxis, and gravitaxis. *T. pyriformis* is a very powerful swimmer and has been shown to be responsive to many stimuli, making it a highly attractive candidate for microrobotic tasks such as microassembling and micromanipulation. This paper focuses on the control of the individual cell rather than a collective group of cells, which is the case with bacteria (Martel et al. 2006; Sakar et al. 2010; Steager et al. 2011). Magnetotaxis is used in our project because of its relative ease of use and effective results. It also does not affect the culture medium unless there are other magnetic materials present. Kim et al. (2009) demonstrated the galvanotactic and phototactic control of *T. pyriformis* as a microfluidic workhorse. Kim et al. (2011) used real-time feedback control and the rapidly-exploring random tree (RRT) for path planning to control the magnetotactic *T. pyriformis* as a microbiorobot. However, this method is not robust when making the cell follow a trajectory with sharp turns and does not take plant model information into account.

Model Predictive Control (MPC) (Carlos et al. 1989; Muske and Rawlings 1993; Li et al. 2005) is an advanced control algorithm widely used in the process control industry. Compared with proportional–integral–derivative (PID) controller, MPC shows its advantages in dealing with time delays and high-order dynamics. Nygaard and Nævdal (2006) presented a nonlinear model predictive control scheme for stabilizing the well pressure during oil well drilling, and Lynch and Bequette (2002) implemented a constrained model predictive controller on a simulated Type-I diabetic patient. However, because of the hardware limitation in the high computational cost, it takes a long time for an MPC controller to solve optimization problems. Therefore, there are only a few studies that focus on implementing MPC in motion control, which requires fast computation for the controller (Poignet and Gautier 2000).

In this paper, the MPC controller is used for the motion control of an artificially magnetotactic *T. pyriformis* as a microbiorobot based on the discrete-time plant model. The research reported in this paper follows our previous work (Ou et al. 2012) and makes three main contributions: First, we derive a discrete-time first principle based model of the plant and measure the plant model parameters by the least-squares method. Second, we use the feedback control with an MPC controller to make *T. pyriformis* follow a predefined track by using an external magnetic field. Third, we use the predictor-like scheme, which executes the

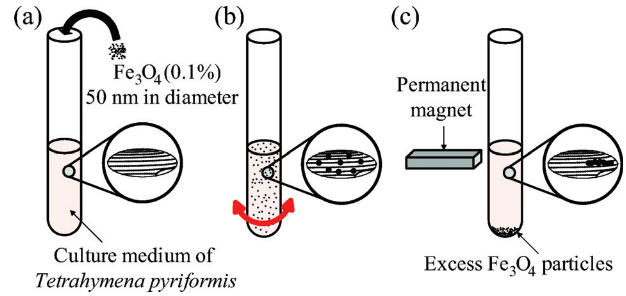

Fig. 1. The procedure for the fabrication of artificially magnetotactic *T. pyriformis*. (a) Addition of iron oxide particles (magnetite, Fe_3O_4) into the culture medium. (b) Gentle agitation to ensure the cells internalize the iron oxide particles. (c) Magnetization of the internalized particles using a permanent magnet. Reproduced from Kim et al. (2011).

plant input before the measurement of the cell position, to deal with the image processing time-delay problem (Asada et al., 2011). In these cases, our theoretical conclusions are confirmed by the experimental validations.

2. Experimental setup

The experiment setup mentioned in this paper is located at the Biological Actuation, Sensing and Transport (BAST) lab at Drexel University, Philadelphia. The same setup was used and reported in our earlier work (Kim et al. 2011; Ou et al. 2012; Wang et al. 2012).

2.1. Cell culture

T. pyriformis was cultured in an appropriate culture medium. The saturated culture has 10^4 cells per mL. The cell culture medium was diluted with a fresh culture medium in a 1 : 3 ratio (the working cell density was 3.3×10^3 cells per mL) in order to lower the cell concentration for single-cell detection.

2.2. Fabrication of artificially magnetotactic T. pyriformis

Figure 1 shows the process that is used to create the artificially magnetotactic *T. pyriformis*. In Figure 1(a), 0.1% iron oxide spherical particles with diameter 50 nm are added to the culture medium. The 50 nm size was chosen so that the nanoparticles could be easily ingested by the cell. In Figure 1(b), the culture medium with iron oxide particles is gently agitated and left for about 10 min to ensure sufficient internalization of the magnetite. The swimming behavior of the magnetite-loaded *T. pyriformis* is identical to normal cells (Rifkin and Ballentine 1976). Figure 1(c) shows that a permanent magnet is applied around the cell culture for about 1 min to magnetize the internalized particles. After magnetization, *T. pyriformis* swims freely without an external magnetic field. Kim et al. (2010) have empirically observed

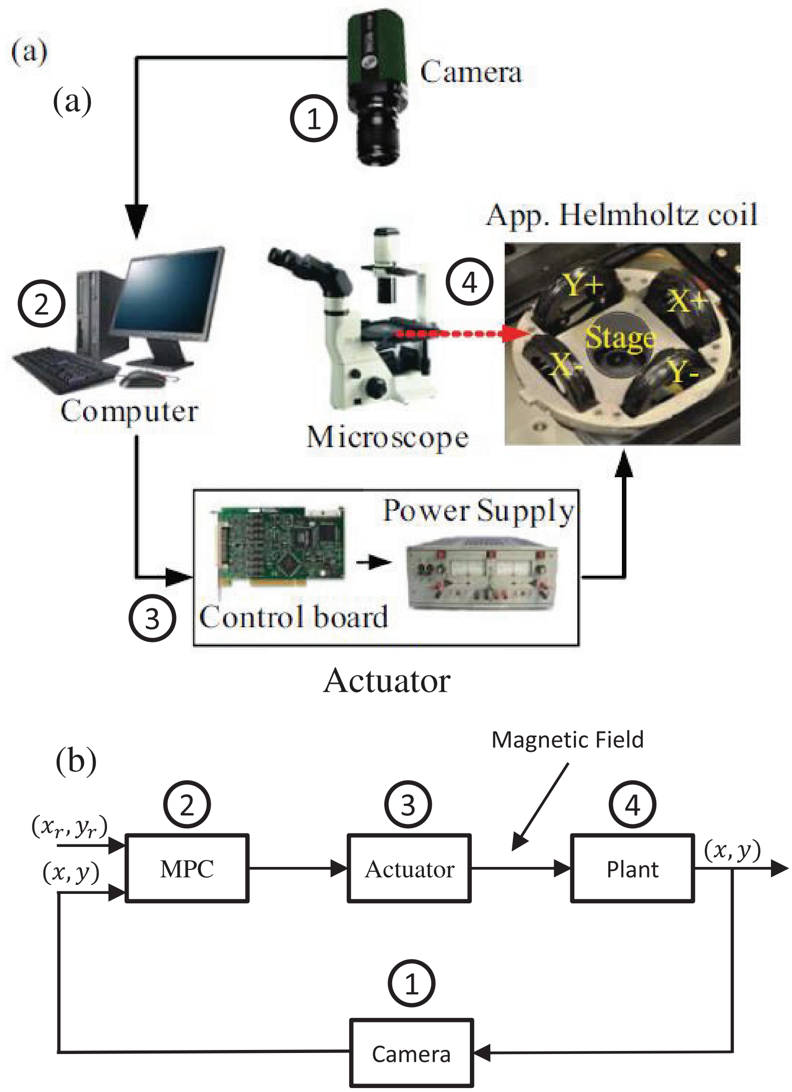

Fig. 2. (a) Experimental setup for feedback control. (b) Control block diagram. In this picture, (x_r, y_r) is the set-point while (x, y) is the cell position. Reproduced from Kim et al. (2011).

that the particles are always aligned with the major axis of the cell. The magnetization of the cells holds for over 1 h after the permanent magnet is removed. It was observed in our experiment that there is no apparent degeneration of the cells' response to the magnetic field. Therefore, it is assumed that the internalized particles are still saturated during the experiments.

2.3. *Closed-loop system*

The system shown in Figure 2(a) is used for the feedback control of magnetotactic *T. pyriformis*, which includes a microscope, a camera, a computer, a control board, two power supplies, and a set of approximate Helmholtz coils. The camera is used to capture images of the cell motion. The computer is used for image processing and the control algorithm. The control board and power supplies provide power to the approximate Helmholtz coils to generate a 2D magnetic field. Within the workspace of size 2 × 2 mm, the magnetic field is approximately constant (Kim et al. 2011). We use a 640×512 pixel video with 2.32 μm/pixel to record the experiment process in this field of view. Figure 2(b) illustrates the control block diagram.

3. Plant Model

3.1. *Structure of the model*

From the data shown in Figure 3, we have empirically discovered that the swimming speed of the cell remains constant regardless of the influence of the external magnetic field. The Helmholtz coils generate an approximately homogeneous magnetic field in the field of view of the microscope, which is limited to 2 mm for each axis (Kim et al. 2011). Once we apply the magnetic field, the angular difference between the magnetic field and the internalized particles produces a torque on *T. pyriformis* to change its moving direction and leads the cells to align with the magnetic field (Kim et al. 2010), shown in Figure 4. In this paper, we generate the plant model by fixing the magnetic field strength while changing the magnetic field angle. Because the experiment is performed in a low Reynolds number fluidic environment, the inertia effect is negligible. Therefore, the relationship between the torque and the angular velocity is approximately linear. We derive the following relation:

$$\tau = \mathbf{m} \times \mathbf{B} = \|\mathbf{m}\| \|\mathbf{B}\| \sin(\theta_t - \theta_{\mathrm{m}}) = -\gamma \dot{\theta}_t, \qquad (1)$$

where γ is constant; $\|\mathbf{m}\|$ is the norm of the magnetic moment; $\|\mathbf{B}\|$ is the norm of the magnetic field; τ is the torque generated by the magnetic field and the magnetic moment; θ_t is the cell angle and θ_{m} is the magnetic field angle. We discretize the continuous-time plant model,

$$\theta_t(k) = \theta_t(k-1) + a_1 \sin(\theta_{\mathrm{m}}(k-1) - \theta_t(k-1)), \qquad (2)$$

$$x(k) = x(k-1) + v(k)\cos(\theta_t(k)), \qquad (3)$$

$$y(k) = y(k-1) + v(k)\sin(\theta_t(k)), \qquad (4)$$

where k represents the time-step; $v(k)$ is the cell position distance between two consecutive sampling time, which is almost constant and can be approximately calculated by averaging the previous 10 steps cell velocities; a_1 is a function of $\|\mathbf{m}\|$, $\|\mathbf{B}\|$, and γ which represents the cell's angular changing rate with respect to the magnetic field. a_1 is different between the cells because of different cell characteristics and different amounts of iron particle internalization; $(x(k-1), y(k-1))$ and $(x(k), y(k))$ are the cell positions.

3.2. Parameter identification

To identify the parameter a_1 for each individual cell, we need to conduct manual control before each automatic control. From the manual control result, we collect the input and output data, $\theta_{\mathrm{m}}(0), \theta_{\mathrm{m}}(1), \ldots, \theta_{\mathrm{m}}(k), \ldots, \theta_{\mathrm{m}}(n)$, and $\theta_t(0), \theta_t(1), \ldots, \theta_t(k), \ldots, \theta_t(n)$. Then, the following equation can be derived based on equation (2):

$$\begin{bmatrix} \theta_t(1) - \theta_t(0) \\ \theta_t(2) - \theta_t(1) \\ \vdots \\ \theta_t(k) - \theta_t(k-1) \\ \vdots \\ \theta_t(n) - \theta_t(n-1) \end{bmatrix} = \begin{bmatrix} \sin(\theta_{\mathrm{m}}(0) - \theta_t(0)) \\ \sin(\theta_{\mathrm{m}}(1) - \theta_t(1)) \\ \vdots \\ \sin(\theta_{\mathrm{m}}(k-1) - \theta_t(k-1)) \\ \vdots \\ \sin(\theta_{\mathrm{m}}(n-1) - \theta_t(n-1)) \end{bmatrix} a_1. \qquad (5)$$

We rewrite this equation as $Y = \Phi a_1$. Based on the least-squares method, the best fit parameter set for the data is given by $a_1^* = \Phi^\dagger Y$ (Bishop 2006; Wang and Boyer 2012), where $\Phi^\dagger = (\Phi^T \Phi)^{-1} \Phi^T$ is the pseudoinverse of Φ.

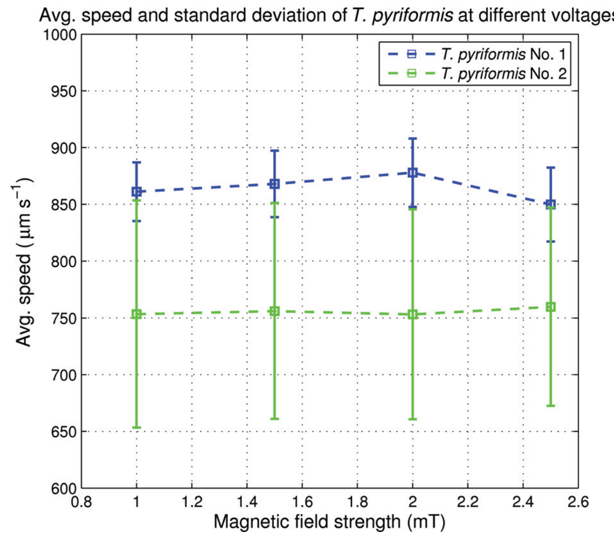

Fig. 3. Comparison of the average speed and the standard deviation between two *T. pyriformis* under the influence of different magnetic field strengths.

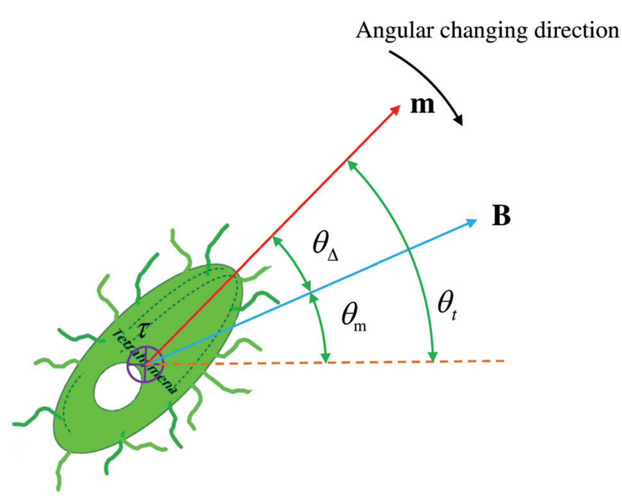

Fig. 4. Mechanical analysis of magnetized *T. pyriformis* under the influence of a magnetic field. In this picture, **B** is the magnetic field; **m** is the magnetic moment; τ is the torque generated by **B** and **m**; θ_t is the cell angle and θ_{m} is the magnetic field angle such that $\theta_\Delta = \theta_t - \theta_{\mathrm{m}}$.

4. MPC Controller design

4.1. Path-generation method

In this paper, we test the control algorithm by making the cell follow different reference tracks. The set-points are generated at each time-step by a heuristic method in order to minimize the distance between the cell's position and the reference track. We explain this method using a simple track that is made up of two lines and two semicircles, as shown in Figure 5. The goal is to make the cell follow this track counterclockwise. From the discrete-time plant model in

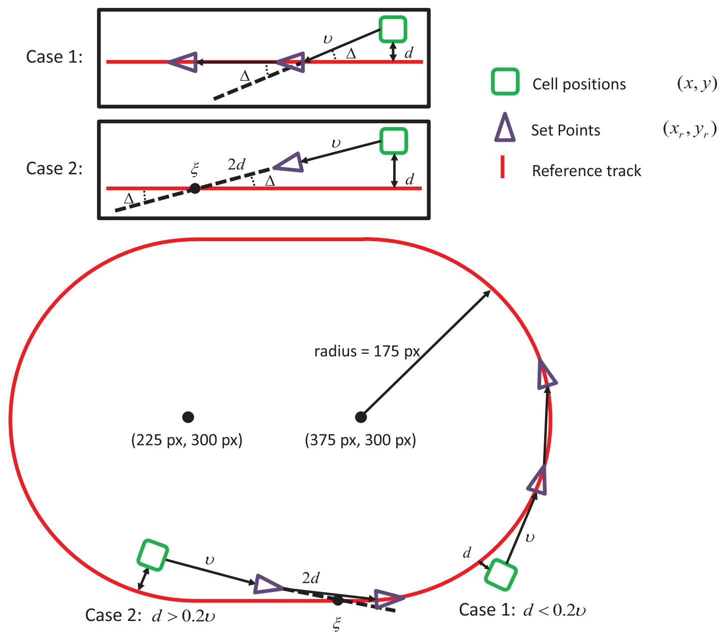

Fig. 5. The reference track and the method to generate the set-points in two different cases. In this picture, the green squares represent the cell positions; the purple triangles represent the set-points; ν is the cell position distance between two consecutive sampling time; d is the distance between *T. pyriformis* and the reference track; ξ is a point in the track with distance $\nu + 2d$ to the cell position; Δ is the angular difference between two step cell positions.

equation (2), we find that there exists a constraint for the change of the cell angle,

$$\theta_t(k-1) - a_1 \leq \theta_t(k) \leq \theta_t(k-1) + a_1. \qquad (6)$$

Figure 5 shows two typical cases in the process of generating set-points. **Case I**: $d < 0.2\nu$. The next set-point can be located on the reference track with distance ν from the current cell position. **Case II**: $d > 0.2\nu$. We choose a position, ξ on the reference track, such that the distance from ξ to the current cell position is $\nu + 2d$. Then we locate the next set-point along the path from the current cell position to ξ with length ν to the current cell position. The threshold value 0.2 is defined heuristically to separate **Case I** from **Case II**. The rule is to generate the set-points with a small angular changing rate, which the cell can follow while satisfying the constraint in equation (6). If the threshold value is set too high, in some cases the angular change of the cell does not satisfy the inequality constraint. If the threshold value is set too low, the cell will fail to follow the reference track rapidly. So the selection of the threshold value is a trade-off. In **Case I**, as is shown in Figure 5, the cell's angular change satisfies the following condition:

$$|\sin(\Delta)| = \frac{d}{\nu} \approx 0.2 < 0.5646 \approx \sin(0.6) \leq \sin(a_1), \quad (7)$$

where Δ is the angular difference between two step cell positions. From the experimental result, a_1 is larger than 0.6 for a well magnetized cell. In **Case II**, as is shown in Figure 5, the cell's angular change satisfies the following condition:

$$\sin(\Delta) \approx \frac{d}{\nu + 2d}. \qquad (8)$$

Equation (8) is a monotonically increasing function with respect to d and $\sin(\Delta) \leq 0.5 < 0.5646 \approx \sin(0.6) \leq \sin(a_1)$. The inequality in equation (6) is still satisfied in this case. Regardless of the above conditions, if the cell's angular changing rate a_1 is set too small, the generated set-points still do not satisfy the inequality constraint in equation (6): i.e. $\theta_t(k) < \theta_t(k-1) - a_1$ or $\theta_t(k) > \theta_t(k-1) + a_1$. We then choose $\theta_t(k) = \theta_t(k-1) - a_1$ or $\theta_t(k) = \theta_t(k-1) + a_1$. During each sampling period, we use this method to generate two consecutive set-points, $(x_r(k+1), y_r(k+1))$ and $(x_r(k+2), y_r(k+2))$.

4.2. MPC Controller

The main goal of the MPC controller is to minimize the cost function in equation (9), which measures the errors between predicted outputs and set-points. As shown by Figure 6, the cost function is formulated as follows:

$$\begin{aligned} J = {} & J_{\mathrm{MPC}}(\theta_{\mathrm{m}}(k), \theta_{\mathrm{m}}(k+1)) \qquad (9)\\ = {} & (x_{\mathrm{p}}(k+1|k) - x_r(k+1))^2 + (y_{\mathrm{p}}(k+1|k) - y_r(k+1))^2 \\ & + (x_{\mathrm{p}}(k+2|k) - x_r(k+2))^2 + (y_{\mathrm{p}}(k+2|k) - y_r(k+2))^2, \end{aligned}$$

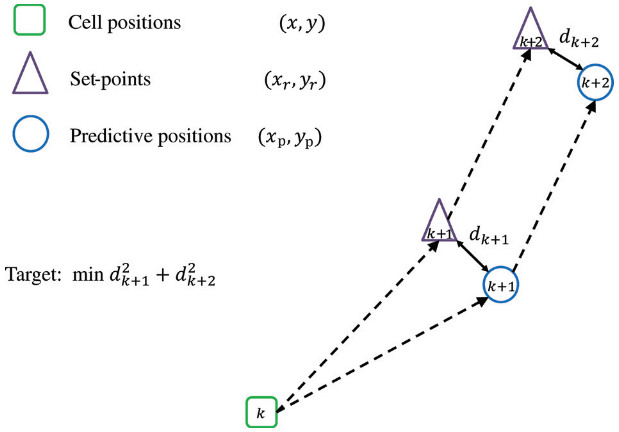

Fig. 6. The main idea of MPC. In this picture, k is the time-step; the green square represents the cell position, which is $(x(k), y(k))$; the purple triangles represent the set-points, which are $(x_r(k+1), y_r(k+1))$ and $(x_r(k+2), y_r(k+2))$; the blue circles represent the predicted positions, which are $(x_p(k+1|k), y_p(k+1|k))$ and $(x_p(k+2|k), y_p(k+2|k))$.

where k is the time-step; $(x_r(k+1), y_r(k+1))$ and $(x_r(k+2), y_r(k+2))$ are the set-points derived from the path-generation method based on the measurement of the k^{th} step cell position $(x(k), y(k))$; $\theta_m(k)$ and $\theta_m(k+1)$ are the magnetic field angles; $(x_p(k+1|k), y_p(k+1|k))$ and $(x_p(k+2|k), y_p(k+2|k))$ are the predicted positions derived from equations (2)–(4) based on the measurement of the k^{th} step cell position $(x(k), y(k))$.

Because the cost function $J_{\text{MPC}}(\theta_m(k), \theta_m(k+1))$ is a non-convex function, we look for a small enough local minimum that substitutes for the global minimum. Equation (2) shows that the cost function is a $2\pi \times 2\pi$ periodic function with respect to $\theta_m(k)$ and $\theta_m(k+1)$, which indicates that the global minimum should appear in the domain $-\pi \leq \theta_m(k) \leq \pi$ and $-\pi \leq \theta_m(k+1) \leq \pi$. We create an 8×8 grid in this domain and execute a Newton iteration search algorithm to find local minima starting from each of the 49 intersections:

$$\Theta_{n+1} = \Theta_n - \left[\frac{\partial^2 J_{\text{MPC}}(\Theta_n)}{\partial \Theta_n^2}\right]^{-1} \frac{\partial J_{\text{MPC}}(\Theta_n)}{\partial \Theta_n}, \tag{10}$$

where $\Theta_n = [\theta_m^n(k), \theta_m^n(k+1)]^T$; n is the Newton iteration step; k is the time-step; $\theta_m(k)$ and $\theta_m(k+1)$ are the magnetic field angles. To approximate the global minimum more precisely, a finer partition can be used. However, it will increase the calculation time. From both the simulation and experimental results, the 8×8 grid separation method has been shown to strike a balance between control performance and time cost.

4.3. Time delay

In the control loop, as shown in Figure 2, the image-processing block and MPC controller block use significant calculation time. In total, there is a nearly 110 ms time delay, which is about one step-sampling time. If we ignore the time delay, the cell will follow the reference track with a large oscillation (Ou et al. 2012), which is shown in Figure 9(a). To deal with the time delay, we use a predictor-like scheme, which is shown in Figure 7. Suppose the iteration is in the k^{th} step, without using this predictor-like scheme, the k^{th} step control input will be obtained and executed at node 3 of this step because of the time delay to get the feedback information and MPC calculation. The predictor-like scheme executes the k^{th} step control input at node 1 of this step without the current step feedback information. The calculation of the k^{th} step control input, completed at node 3 of the $(k-1)^{\text{th}}$ step, predicts one step cell information ahead. Also, the $(k+1)^{\text{th}}$ step control input is executed at node 1 of the $(k+1)^{\text{th}}$ step and obtained at node 3 of the k^{th} step. Regarding the predictor-like scheme, we rewrite equation (9) to obtain:

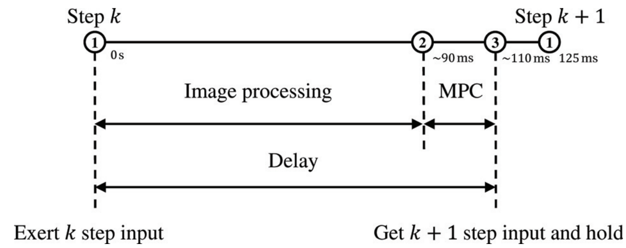

Fig. 7. Delay problem. In this picture, the image-processing calculation costs about 90 ms; the MPC controller calculation costs about 20 ms; the sampling time is 125 ms; k is the time-step.

$$\begin{aligned} J &= J_{\text{MPC}}(\theta_m(k+1), \theta_m(k+2)) \\ &= (x_p(k+2|k) - x_r(k+2))^2 + (y_p(k+2|k) - y_r(k+2))^2 \\ &\quad + (x_p(k+3|k) - x_r(k+3))^2 + (y_p(k+3|k) - y_r(k+3))^2, \end{aligned} \tag{11}$$

where k is the time-step; $(x_p(k+2|k), y_p(k+2|k))$ and $(x_p(k+3|k), y_p(k+3|k))$ are the predicted positions derived from equations (2)–(4) based on the measurement of the k^{th} step cell position $(x(k), y(k))$; $(x_r(k+2), y_r(k+2))$ and $(x_r(k+3), y_r(k+3))$ are the set-points derived from the path-generation method based on the $(k+1)^{\text{th}}$ step predicted cell position $(x_p(k+1|k), y_p(k+1|k))$; $\theta_m(k+1)$ and $\theta_m(k+2)$ are the magnetic field directions.

4.4. Algorithm

The MPC controller that takes the time delay into account is presented in Algorithm 1.

5. Results

5.1. Manual control

We conducted our experiments in a polydimethylsiloxane (PDMS) channel. The PDMS channel was fabricated with a depth of 80 μm to give the cells sufficient space to swim

Algorithm 1 The MPC strategy

Compute a_1 based on the captured manual control data.
for $k = 1, 2, 3, \ldots$ **do**
  execute $\theta_\mathrm{m}(k)$ before image processing.
  Get $(x(k), y(k))$ from image processing.
  Calculate $v(k)$ by averaging the previous 10 steps' cell speed.
  Compute $\theta_t(k)$ using equations (3)–(4) which satisfy $\theta_t(k) \in [\theta_t(k-1) - \pi, \theta_t(k-1) + \pi]$.
  Predict three future steps cell positions, $(x_\mathrm{p}(k+1|k), y_\mathrm{p}(k+1|k))$, $(x_\mathrm{p}(k+2|k), y_\mathrm{p}(k+2|k))$ and $(x_\mathrm{p}(k+3|k), y_\mathrm{p}(k+3|k))$, based on $(x(k), y(k))$ and the plant model.
  Generate the $k+2$ and $k+3$ step set-points, $(x_r(k+2), y_r(k+2))$ and $(x_r(k+3), y_r(k+3))$ based on $(x_\mathrm{p}(k+1|k), y_\mathrm{p}(k+1|k))$ and the path-generation method.
  Build cost function $J_\mathrm{MPC}(\theta_\mathrm{m}(k+1), \theta_\mathrm{m}(k+2))$ to measure the error between the predicted positions and the set-points in $k+2$ and $k+3$ steps.
  Use the Newton iteration method from different initial values in the domain to find a small enough local minimum $(\theta_\mathrm{m}(k+1), \theta_\mathrm{m}(k+2))$, which substitutes for the global minimum of the cost function.
  Hold $\theta_\mathrm{m}(k+1)$ until the beginning of the $(k+1)^\mathrm{th}$ step.
end for

freely. The magnetic field angle was manually changed in both positive and negative directions on either the x- or the y-axis using four arrow keys on a standard PC keyboard. Based on Persistent Excitation (PE) condition (Ioannou and Sun 1995) to ensure the convergence of a_1, the input signal should contain enough frequencies. In this case, we chose a nonperiodic rectangular wave as an input. Figure 8 shows a good match between the estimated result and the experimental result. From this experimental data, we obtained the optimal parameter $a_1^* = 0.6665$.

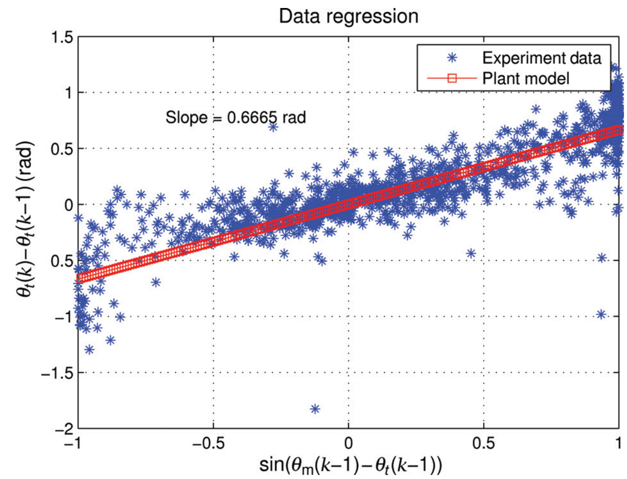

Fig. 8. Data regression of equation (2). In this picture, the blue dots are the experimental data, while the red squares represent the regression line with slope 0.6665 rad.

5.2. Automatic control

In the experiment, a single *T. pyriformis* cell is manually controlled for 11 s to get enough data for parameter identification. Once the plant parameter a_1 is generated by the least-squares method, the MPC controller will be activated to automatically control the cell to follow the reference track. The sampling time of the whole system is set to be 125 ms (8 Hz), which is longer than the delay time of the system.

5.2.1. Comparison I: MPC without considering the delay vs. MPC with consideration of the delay In Figure 9(a), by using the MPC without considering the delay, the cell follows the reference track with a large error and oscillation. However in Figure 9(b), when the delay is taken into account and the predictor-like scheme is used, the cell follows the reference track much more accurately. Figure 9(c) and (d) show the distribution of distances between the cell positions and the reference track. For the MPC without considering the delay, the mean value of the distance is 26.2727 μm and the standard deviation is 48.7748 μm, which means that the average position of the cell is outside the track and there is a relatively large standard deviation of the cell positions. For the MPC with this predictor-like scheme, the mean value of the distance is −5.9778 μm and the standard deviation is 16.1632 μm. Thus we conclude that the average position of the cell is inside the track with a small error and the standard deviation is also relatively small.

5.2.2. Comparison II: Weak magnetic field vs. strong magnetic field If the magnetic field strength increases, the cell will have a larger angular changing rate. Therefore, we are able to make the cell turn faster. Here, a narrower track has been chosen as the reference track. During the experiment, the magnetic field strengths are kept constant in both the weak magnetic field case and the strong magnetic field case. In Figure 10(a), the cell follows the reference track in a weak magnetic field with a large error in the sharp turn. This is because the angular changing rate of the cell is too small ($\|\mathbf{B}\| = 1$ mT and $a_1 = 0.4885$). In Figure 10(b), the cell follows the reference track more accurately in the strong magnetic field case ($\|\mathbf{B}\| = 3$ mT and $a_1 = 0.6663$). Figure 10(c) and (d) show the distribution of distances between cell positions and the reference track. For the weak magnetic field case, the mean value of the distance is 44.4572 μm and the standard deviation is 58.4643 μm, which means that the average position of the cell is outside the track and the standard deviation is relatively large. For the strong magnetic field case, the mean value is −17.3684 μm and the standard deviation is 17.0951 μm, which means that the average

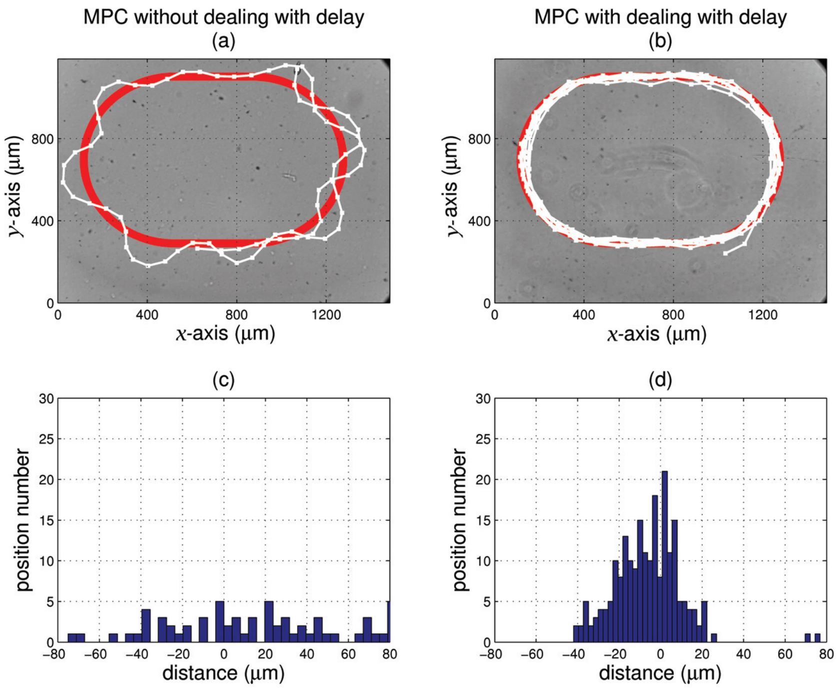

Fig. 9. Comparison I. (a) and (b) Trajectory tracing. The red stars represent the reference track; the white square line is the cell motion trajectory. (c) and (d) The distribution of the distance between the cell positions and the reference track. Negative distance means the cell is inside the track; positive distance means the cell is outside the track. In (c), the mean value is 26.2727 μm and the standard deviation is 48.7748 μm; while in (d), the mean value is −5.9778 μm and the standard deviation is 16.1632 μm.

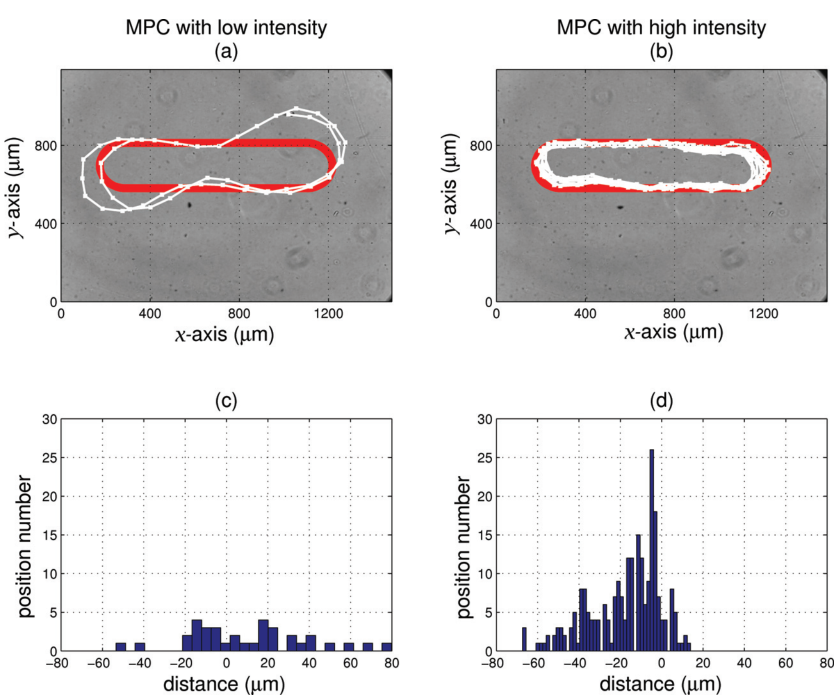

Fig. 10. Comparison II. (a) and (b) Trajectory tracing. The red stars represent the reference track; the white square line is the cell motion trajectory. (c) and (d) The distribution of the distance between the cell positions and the reference track. Negative distance means the cell is inside the track; positive distance means the cell is outside the track. In (c), the mean value is 44.4572 μm and the standard deviation is 58.4643 μm; while in (d), the mean value is −17.3684 μm and the standard deviation is 17.0951 μm.

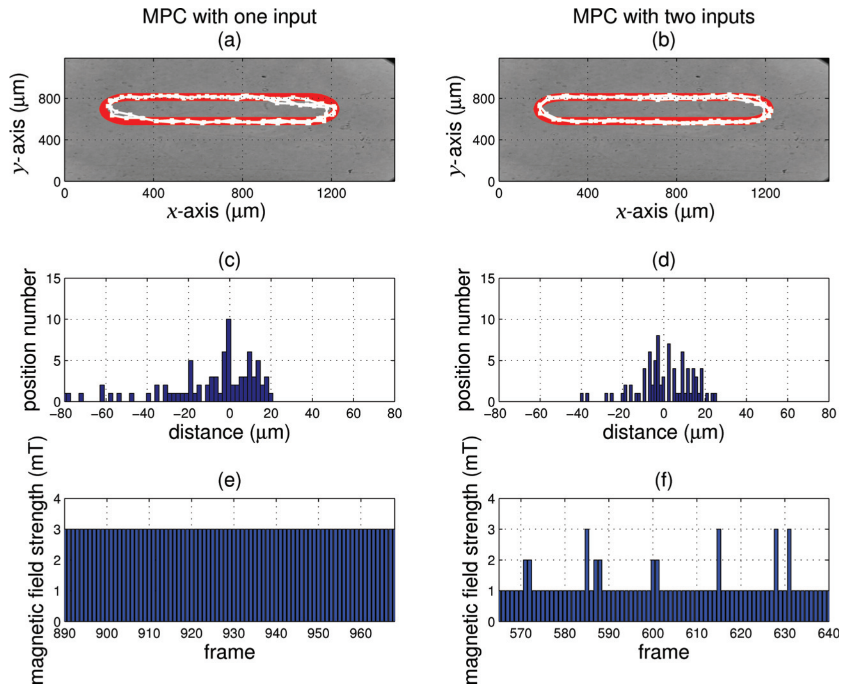

Fig. 11. Comparison III. (a) and (b) Cell follow trajectory. The red stars represent the reference track; the white square line is the cell motion trajectory. (c) and (d) Distribution of distances between the cell positions and the reference track. Negative distance means that the cell position is inside the track; positive distance means that the cell position is outside the track. In (c), the mean value is 9.0702 μm and the standard deviation is 23.4367 μm; while in (d), the mean value is −0.7442 μm and the standard deviation is 13.1386 μm. (e) and (f) Magnetic field strength values during the experiment. In (e), the average magnetic field strength is 3 mT, while in (f), the average magnetic field strength is 1.1728 mT.

position of the cell is inside the track with a small error and the standard deviation is also relatively small.

5.2.3. Comparison III: One input control vs. two input controls As mentioned above, the cell speed is practically constant during the experiments. In the case that the cell moves along a straight line, using the strong magnetic field for the experiment is not a power-saving practice. Therefore, we can use the high magnetic field strength in the sharp turn while using the low magnetic field strength in the straight line. In this case, the magnetic field strength is another input to control the cell. By using the two input controls, magnetic field strength and magnetic field angle, the cell can be controlled to follow the reference track with low energy consumption. From equation (2), for the same cell, a_1 depends mainly on the magnetic field strength, $\|\mathbf{B}\|$, because $\|\mathbf{m}\|$ and γ are kept constant. In this case, we need to calculate a different a_1 for each magnetic field strength. We use the batch least-squares method to identify the a_1. In the experiment shown in Figure 11, $a_1 = 0.6777$ in a 1 mT magnetic field; $a_1 = 0.8676$ in a 2 mT magnetic field; $a_1 = 1.0726$ in a 3 mT magnetic field. In general, a_1 monotonically increases with respect to the magnetic field strength. In equation (2), if a_1 is larger, the cell can make a larger turn. In each automatic control time-step, we choose a_1 in a 3 mT magnetic field as the constraint of the cell's angular change in equation (6) to generate the set-points. Then, a simplified MPC algorithm is used to obtain the control inputs θ_{m} and T_{m}. We define the optimization strategy $E(T_{\mathrm{m}})$ as:

$$E(T_{\mathrm{m}}) = \min_{\theta_{\mathrm{m}}(k+1)} \left(\theta_{\mathrm{p}}(k+2) - \theta_r(k+2)\right)^2, \qquad (12)$$

where $\theta_{\mathrm{p}}(i+1) = \theta_{\mathrm{p}}(i) + a_1(T_{\mathrm{m}}(i)) \sin(\theta_{\mathrm{m}}(i) - \theta_{\mathrm{p}}(i))$, $i = k, k+1$; θ_{m} is the magnetic field angle while T_{m} is the magnetic field strength. Then T_{m} is chosen by $\min_{T_{\mathrm{m}}} \{E(T_{\mathrm{m}}) = 0\}$. Based on this method, the high magnetic field strength is chosen to make the cell follow the sharp turn part of the reference track while the low magnetic field strength is chosen to make the cell follow the straight line part. In Figure 11(a) and (b), the trajectories of the cells are quite similar between the one-input MPC and the two-input MPC. Figure 11(c) and (d) show the distribution of distances between cell positions and the reference track. For the one-input MPC, the mean value of the distance is 9.0702 μm and the standard deviation is 23.4367 μm; while for the two-input MPC, the mean value is −0.7442 μm and the standard deviation is 13.1386 μm. Figure 11(e) and (f) show the magnetic field strength of the one-input MPC and the two-input MPC. For the one-input MPC, the average magnetic field strength is 3 mT; while for the two-input MPC, the average magnetic field strength is 1.1728 mT.

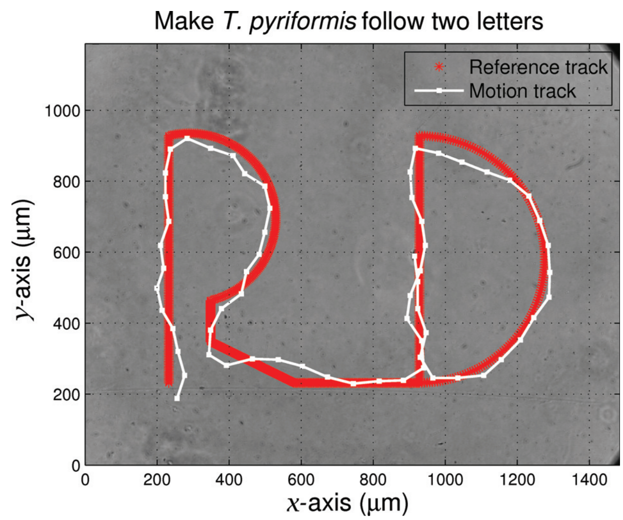

Fig. 12. Initials tracing. In this picture, the red stars represent the reference track; the white square line is the cell motion trajectory.

5.2.4. Initials tracing Figure 12 shows the two initial letters "R" and "D" for Rensselaer Polytechnic Institute and Drexel University respectively. These two letters contain straight lines, sharp turns, and smooth turns to test the performance of MPC. In this experiment, we steer the cell to trace the letters. The magnetic field strength is fixed to 2 mT. The cell follows the trajectory quite well with a minor error in the sharp turn of the letter "R".

6. Conclusions

In this paper, we discuss the use of MPC in the motion control of magnetotactic *T. pyriformis* by a magnetic field. Based on the discrete-time plant model of magnetotactic *T. pyriformis* under the influence of an external magnetic field, the plant parameter is generated using manual control data and the least-squares method. The model is then used in the feedback control. To deal with the image-processing delay, we use a predictor-like scheme to execute input ahead of the measurement of the cell position. In the result section, we show three comparisons between different control schemes and an initial tracking to prove the effectiveness of the control approach.

Funding

This work was partially supported by NSF CMMI Control Systems (grant numbers 1000284 and 1000255) and the Army Research Office (grant number W911NF1110490).

References

Abbott J, Nagy Z, Beyeler F and Nelson B (2007) Robotics in the small, part I: microbotics. *IEEE Robotics & Automation Magazine* 14(2): 92–103.

Asada HH, Wang Y and Mayalu MN (2011) Molecular signaling observer and predictor: A framework for closed-loop control of cell behaviors having long time delay. In: *2011 american control conference*, San Francisco, USA, 29 June – 1 July 2011, pp. 2314–2319. Piscataway: IEEE Press.

Bishop CM (2006) *Pattern Recognition and Machine Learning*. New York: Springer-Verlag.

Carlos EG, David MP and Manfred M (1989) Model predictive control: theory and practice–a survey. *Automatica* 25(3): 335–348.

Donald BR, Levey CG and Paprotny I (2008) Planar microassembly by parallel actuation of MEMS microrobots. *Journal of Microelectromechanical Systems* 17(4): 789–808.

Fearing RS (1991) Control of a micro-organism as a prototype micro-robot. In: *2nd international symposium on micromachines and human sciences*, Nagoya, Japan, 8-9 October 1991.

Hunter IW, Lafontaine S, Nielsen PMF, Hunter PJ and Hollerbach JM (1990) Manipulation and dynamic mechanical testing of microscopic objects using a tele-micro-robot system. *IEEE Control Systems Magazine* 10(2): 3–9.

Ioannou PA and Sun J (1995) *Robust Adaptive Control*. Mineola: Dover Publications.

Itoh A (2000) Motion control of protozoa for bio-MEMS. *IEEE/ASME Transactions on Mechatronics* 5(2): 181–188.

Itoh A, Tamura W and Mishima T (2005) Motion control of euglena group by weak laser scanning system and object manipulation using euglena group. In: *IEEE/ASME international conference on advanced intelligent mechatronics*, Monterey, California, USA, 24–28 July 2005, pp. 43–47. Piscataway: IEEE Press.

Itoh A and Toida H (2001) Control of bioconvection and its mechanical application. In: *IEEE/ASME international conference on advanced intelligent mechatronics*, Como, Italy, 8–12 July 2001, vol. 2, pp. 1220–1225. Piscataway: IEEE Press.

Julius AA, Sakar MS, Steager E, Cheang UK, Kim MJ, Kumar V et al. (2009) Harnessing bacterial power in microscale actuation. In: *IEEE international conference on robotics and automation (ICRA '09)*, Kobe, Japan, 12–17 May 2009, pp. 1004–1009. Piscataway: IEEE Press.

Kim DH, Brigandi S, Julius AA and Kim MJ (2011) Real-time feedback control using artificial magnetotaxis with rapidly-exploring random tree (RRT) for *Tetrahymena pyriformis* as a microbiorobot. In: *IEEE international conference on robotics and automation (ICRA '11)*, Shanghai, China, 9–13 May 2011, pp. 3183–3188. Piscataway: IEEE Press.

Kim DH, Casale D, Köhidai L and Kim MJ (2009) Galvanotactic and phototactic control of *Tetrahymena pyriformis* as a microfluidic workhorse. *Applied Physics Letters* 94(16): 163901.

Kim DH, Cheang UK, Köhidai L, Byun D and Kim MJ (2010) Artificial magnetotactic motion control of *Tetrahymena pyriformis* using ferromagnetic nanoparticles: A tool for fabrication of microbiorobots. *Applied Physics Letters* 97(17): 173702.

Li S, Zhang Y and Zhu Q (2005) Nash-optimization enhanced distributed model predictive control applied to the Shell benchmark problem. *Information Sciences* 170(2–4): 329–349.

Lynch S and Bequette B (2002) Model predictive control of blood glucose in type I diabetics using subcutaneous glucose measurements. In: *2002 american control conference*, Anchorage, Alaska, USA, 8–10 May 2002, vol. 5, pp. 4039–4043. Piscataway: IEEE Press.

Martel S (2006) Targeted delivery of therapeutic agents with controlled bacterial carriers in the human blood vessels. In: *2006 bio micro and nanosystems conference (BMN '06)*, Montreal, Canada, 15–18 January 2006, p. 9. Piscataway: IEEE Press.

Martel S, Mohammadi M, Felfoul O, Zhao L and Pouponneau P (2009) Flagellated magnetotactic bacteria as controlled MRI-trackable propulsion and steering systems for medical nanorobots operating in the human microvasculature. *International Journal of Robotics Research* 28(4): 571–582.

Martel S, Tremblay CC, Ngakeng S and Langlois G (2006) Controlled manipulation and actuation of micro-objects with magnetotactic bacteria. *Applied Physics Letters* 89(23): 233904.

Muske KR and Rawlings JB (1993) Model predictive control with linear models. *AIChE Journal* 39: 262–287.

Nygaard G and Nævdal G (2006) Nonlinear model predictive control scheme for stabilizing annulus pressure during oil well drilling. *Journal of Process Control* 16(7): 719–732.

Ou Y, Kim DH, Kim P, Kim MJ and Julius AA (2012) Motion control of *Tetrahymena pyriformis* cells with artificial magnetotaxis: model predictive control (MPC) approach. In: *IEEE international conference on robotics and automation (ICRA '12)*, St. Paul, USA, 14–18 May 2012, pp. 2492–2497. Piscataway: IEEE Press.

Pawashe C, Floyd S and Sitti M (2009) Multiple magnetic microrobot control using electrostatic anchoring. *Applied Physics Letters* 94(16): 164108.

Poignet P and Gautier M (2000) Nonlinear model predictive control of a robot manipulator. In: *6th international workshop on advanced motion control*, Nagoya, Japan, 30 March – 1 April 2000, pp. 401–406. Piscataway: IEEE Press.

Rifkin JL and Ballentine R (1976) Magnetic fettering of the ciliated protozoon *Tetrahymena pyriformis*. *Transactions of the American Microscopical Society* 95(2): 189–197.

Sakar MS, Steager EB, Kim DH, Kim MJ, Pappas GJ and Kumar V (2010) Single cell manipulation using ferromagnetic composite microtransporters. *Applied Physics Letters* 96(4): 043705.

Steager EB, Sakar MS, Kim DH, Kumar V, Pappas GJ and Kim MJ (2011) Electrokinetic and optical control of bacterial microrobots. *Journal of Micromechanics and Microengineering* 21(3): 035001.

Wang Q and Boyer KL (2012) The active geometric shape model: A new robust deformable shape model and its applications. *Computer Vision and Image Understanding* 116(12): 1178–1194.

Wang Q, Ou Y, Julius AA, Boyer KL and Kim MJ (2012) Tracking *Tetrahymena Pyriformis* cells using decision trees. In: *21st international conference on pattern recognition*, Tsukuba, Japan, 11–15 November 2012.

Weibel DB, Garstecki R, Ryan D, DiLuzio WR, Mayer M, Seto JE et al. (2005) Microoxen: microorganisms to move microscale loads. *Proceedings of the National Academy of Sciences* 102(34): 11963–11967.

Yi T, Huang Y, Simon MI and Doyle J (2000) Robust perfect adaptation in bacterial chemotaxis through integral feedback control. *Proceedings of the National Academy of Sciences* 97(9): 4649–4653.

Zhang L, Abbott JJ, Dong L, Kratochvil BE, Zhang H, Peyer KE et al. (2009) Micromanipulation using artificial bacterial flagella. In: *IEEE/RSJ international conference on intelligent robots and systems (IROS '09)*, St. Louis, USA, 11–15 October 2009, pp. 1401–1406. Piscataway: IEEE Press.